

Numerical Study of Energy Deposits in Superconducting Magnet Coils

Logan Maingi
Fermilab National Accelerator Laboratory

August 13, 2010

Abstract

The energy deposition map is one of the essential Network Model inputs. A Network Model is used to study the thermodynamic behavior of magnet coils and to calculate the quench levels in the superconducting magnets for expected beam loss profiles (energy deposits). In order to prepare the input to Network Model an interface between FLUKA or MARS output and Network Model is needed. This paper describing the 2D interpolation of energy deposition map from FLUKA or MARS onto the coordinates of magnet coil conductors. The study if two magnet cross-sections at different bin z have heat loads that display an approximate linear relationship was also performed.

1 Introduction

1.1 Background

Magnet quenching in the LHC [1] is undesirable, so one would like to minimize the number of quenches. In order to do so, one needs to calculate the quench limit of each proposed magnet design. The magnet quench during accelerator operation can be provoked by energy deposited in the superconductor by the particle beams [2, 3]. In particular, particles impacting on the vacuum chamber and their secondary showers deposit energy in the magnet coils [4]. In order to calculate the energy depositions, Monte Carlo simulations, namely MARS [5, 6] and FLUKA [7, 8], were used to model particle interaction and transport.

Typically these codes homogenize the magnet and calculate energy depositions in some standard coordinate system. However, for certain applications, including computing the thermodynamics of the magnet, energy depositions in each of the individual conductors are needed for precise computations. The coordinates of these conductors do not, in general, correspond to the coordinates output by FLUKA and MARS (see figure 1), so interpolation is necessary. In particular, the network model for heat transfer [9, 10] requires such interpolation.

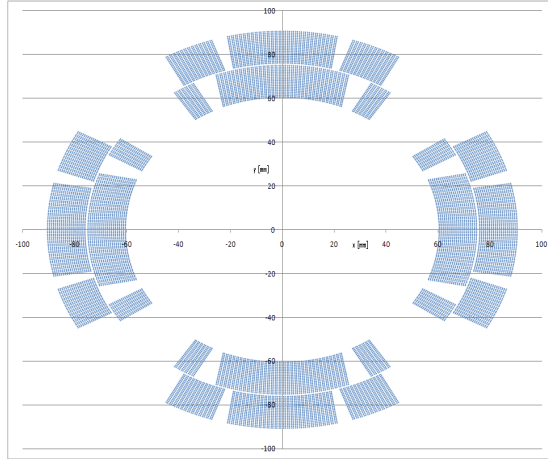


Figure 1: *Diagram of the conductors in one proposed quadrupole magnet.*

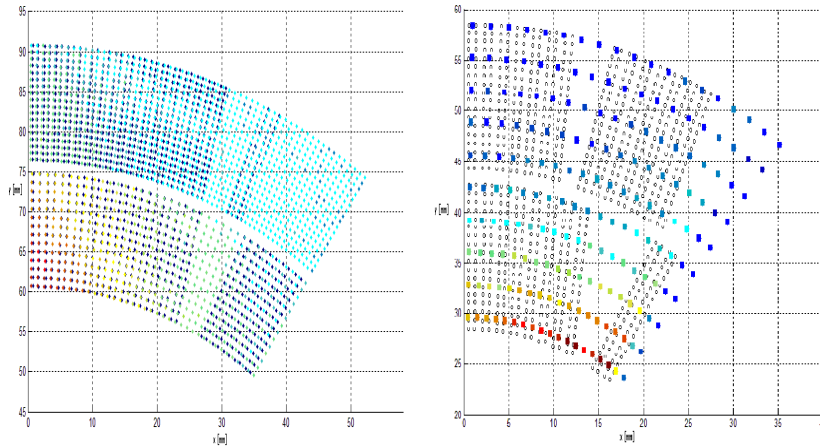


Figure 2: *Closeup of partial coordinates of magnets vs coordinates of FLUKA simulations in 2 cases. Left: Colored points are FLUKA data points, and the color indicates the energy deposition. Dark blue points indicate conductor coordinates. Right: Empty circles indicate conductors.*

For high resolution simulations of the energy depositions, a simple interpolation method, such as nearest neighbor or linear interpolation will suffice. However, if the output data is lower resolution, more advanced nonlinear methods may be necessary. The left plot in figure 2 shows a FLUKA simulation with tight binning and less need for interpolation; the right plot shows a low resolution binning scheme in which interpolation is more important.

The most challenging aspect of preparing a model for the energy deposition map is that the energy depositions are 3-dimensional and complicated, with several maxima at different levels for each longitudinal plane. One way to deal with this is to attempt to find an interdependence between different the energy depositions at different longitudinal cross-sections. The simplest method is to find a linear relationship between the energy deposits in any two longitudinal bins. Such a relationship would reduce the difficulty of performing analysis on the energy deposition map.

1.2 Project Description

Two 2-dimensional interpolation routines for one longitudinal bin namely a bilinear method and a bicubic method, were written. This was extended to a 3-dimensional routine by locating the cross-section with greatest energy deposits and interpolating on this. This routine works for both FLUKA and MARS outputs. These methods were used to interpolate the energy deposition maps from FLUKA and MARS onto the ROXIE [11, 12] conductor coordinates for the magnet.

Based on these data, the nature of the energy deposition maps was studied. In particular, it was observed how close to linearly proportional the heat loads are for any two longitudinal bins. This was accomplished through use of both statistical analysis and graphical techniques.

2 Interpolation

2.1 2-Dimensional Interpolation in FLUKA

The output data from FLUKA are given as a regular grid in polar coordinates, which does not correspond to the conductor coordinates from ROXIE. To alleviate this, we must interpolate the energy deposition map from FLUKA onto the coordinates of the conductors.

2.1.1 Bilinear Interpolation

The first interpolant we consider, which is the simplest nontrivial interpolant in 2 dimensions, is a bilinear method:

Definition 1 *Suppose $E(r, \phi)$ is a function of two variables whose values are known on a finite grid*

$$\Lambda = \{r_i = r_0 + i\Delta r \mid i = 0, \dots, m-1\} \times \{\phi_j = \phi_0 + j\Delta\phi \mid j = 0, \dots, n-1\}$$

in polar coordinates, where $\Delta\phi = \frac{2\pi}{n}$ to ensure 2π -periodicity of ϕ . We define the polar bilinear interpolant $L_E(r, \phi)$ by the following:

For $(r, \phi) \in [r', r' + \Delta r) \times [\phi', \phi' + \Delta\phi)$, where $(r', \phi') \in \Lambda$, let

$$L_E(r, \phi) := \left(\frac{r' + \Delta r - r}{\Delta r} \right) \left(\frac{\phi' + \Delta\phi - \phi}{\Delta\phi} \right) E(r', \phi') + \left(\frac{r - r'}{\Delta r} \right) \left(\frac{\phi' + \Delta\phi - \phi}{\Delta\phi} \right) E(r' + \Delta r, \phi') \\ + \left(\frac{r' + \Delta r - r}{\Delta r} \right) \left(\frac{\phi - \phi'}{\Delta\phi} \right) E(r', \phi' + \Delta\phi) + \left(\frac{r - r'}{\Delta r} \right) \left(\frac{\phi - \phi'}{\Delta\phi} \right) E(r' + \Delta r, \phi' + \Delta\phi).$$

Bilinear interpolation is the simplest 2-dimensional interpolation method other than nearest-neighbor interpolation, which is not particularly useful. Qualitatively, the method assigns $L_E(r, \phi)$ based on its 4 nearest neighbors in such a way that $L_E(r, \theta)$ is a linear function in r for any θ and $L_E(s, \phi)$ is a linear function in ϕ for any s . It provides a continuous interpolant. Because it depends not only on r and ϕ linearly, but also has a linear dependence on their product $r\phi$, the method is actually quadratic, but as $L_E(r, \phi)$ can be written as a product of linear functions in r and in ϕ , it is known as a bilinear interpolant.

A bilinear interpolation method was written to take the regularly gridded output from FLUKA and output the interpolated energy deposition values at the various conductor positions. This method is flexible enough to work with different numbers of bins in r and ϕ , i.e. different values of m and n . Because FLUKA data for the inner and outer layers of the magnet is separate, it also accommodates this by first checking which region the desired point is in, then interpolating in that region.

Procedure This procedure takes FLUKA output energy deposition data and magnet coordinates from ROXIE as its inputs. The procedure iterates on the rows of the ROXIE coordinates file. For each conductor, the interpolation procedure computes the position (r, ϕ) of the conductor from the given (x, y) . By testing the value of r and comparing this to the values in the inner and outer layers, it determines which region the point falls into. After this, it uses the data only from that region.

From the given (r, ϕ) , the quantity $\frac{r-r_0}{\Delta r}$ is computed. The integer part of this indicates the FLUKA radial bin r_i to be used for r' selected as the lower bound of the region; r_{i+1} is the upper radial bound. In the case that $i < 0$ or $i > m - 2$, interpolation is not technically possible, but by forcing $i = 0$ or $i = m - 2$, a decent extrapolation can be achieved. $\phi' = \phi_j$ is calculated the same way, except that rather than forcing extrapolation in this case, we exploit the periodicity of ϕ near the edge.

2.1.2 Bicubic Interpolation

Bilinear interpolation works by fitting the 4 nearest known points to a product of linear functions. Likewise, bicubic interpolation works by fitting 16 nearby points to a product of cubic functions. This is a more general method than bilinear expansion, and is expected to be more accurate.

Definition 2 Take everything as in the definition of the bilinear interpolant. Then the bicubic interpolant is defined piecewise as the unique function $C_E(r, \phi)$

which is of the form $\sum_{e=0}^3 \sum_{f=0}^3 c_{e,f} r^e \phi^f$ for $(r, \phi) \in [r', r' + \Delta r) \times [\phi', \phi' + \Delta \phi)$

where $c_{e,f}$ are coefficients determined so that $\sum_{e=0}^3 \sum_{f=0}^3 c_{e,f} r^e \phi^f = E(r, \phi)$ for $(r, \phi) = (r' + k\Delta r, \phi' + l\Delta \phi)$, where $k, l = -1, 0, 1, 2$

This definition has an obvious generalization for any 2D polynomial interpolation, which includes the bilinear case. The coefficients can be solved for, as in the bilinear case, as a linear function of the known values of E . Higher orders of polynomial interpolants are also possible, but tend to have too many free parameters to be useful.

This method's most important feature is its nonlinearity, as the energy depositions are known to be nonlinear at some level. Because the grids we have are not in general high-resolution, there is reason to believe that more advanced methods will not produce any better results, and may indeed be a burden due to phenomena associated with interpolating with large numbers of model parameters.

Procedure The same procedure is followed from the linear interpolation, excluding some modifications. The inputs are all taken the same as in the case of linear interpolation. Bicubic interpolation requires 16 points around the desired interpolation point, rather than the 4 points for bilinear interpolation. As such, $i \geq 1$ and $i \leq m - 3$ are needed, rather than in the above case. However, it is noted in practice that bicubic expansion behaves poorly near the edge of the data set, causing undesirable artifacts. As such, rather than extrapolating in the case these conditions are not met, the code defaults to linear extrapolation for that particular point.

The only other significant difference in the computation of $C_E(r, \phi)$ from $L_E(r, \phi)$ is how the coefficients are chosen. These are given by a 16×16 matrix expression [13]. The problem then reduces to evaluating the matrix product, and evaluating the cubic interpolant.

2.1.3 Results

The results of both interpolation procedures was as expected (see figures 3-5). Both were able to interpolate accurately avoiding undesirable behavior in most of the magnet. Very near the edge of the magnet, the bicubic interpolation—a 6th order method—behaves somewhat poorly due to Runge's phenomenon and lack of useful interpolating data. As such, it was decided that in this region, the bicubic method would be substituted by the bilinear method.

The difference in the methods is at maximum approximately 10% of the energy deposition in that region (see figure 5). This is considered an acceptable level, given that the FLUKA code has error on the order of a factor of 2 due

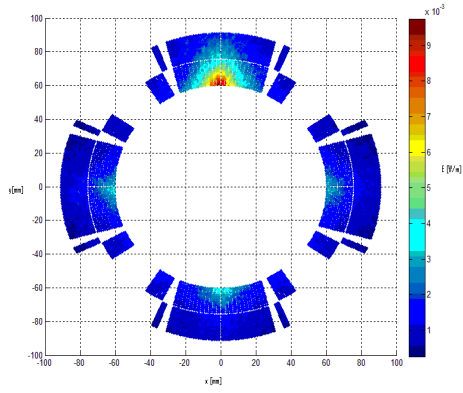


Figure 3: Plot of result from using a bilinear interpolant on the FLUKA output data.

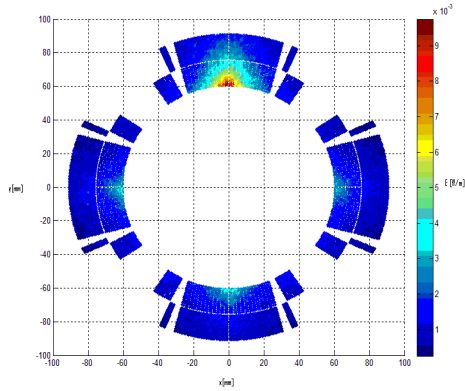


Figure 4: Plot of result from using a bicubic interpolant on the FLUKA output data.

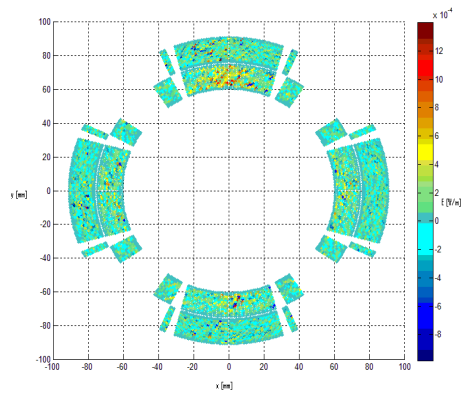


Figure 5: Plot of the difference $L_E(r, \phi) - C_E(r, \phi)$. Note the scale difference between this and the previous two plots.

to uncertainty associated with particle production and other random effects. The performance speed of both codes was not an issue, so bicubic interpolation proved the better of the two methods for future use.

2.2 Interpolation on MARS Simulations

MARS does similar calculations to FLUKA, but with a different method giving energy depositions per unit mass instead of per unit volume. By using the density of the magnet, these can easily be converted to the desired units. They provide a cross-check for each other, as they use different methods but end with the same results[14]. The major difference between FLUKA and MARS output for the purposes of interpolation is that FLUKA uses cylindrical coordinates, while MARS gives results in Cartesian coordinates.

Unlike in the case of FLUKA, for MARS, the simulation region extends far past the magnet in all directions. As such it is not necessary to extrapolate and/or use linear in the place of cubic interpolation, as data surrounding the desired location is abundant.

The replacement of polar (r, ϕ) coordinates with Cartesian (x, y) coordinates is in practice of little significance. If anything, because x and y are symmetric, the code is expected to perform slightly better with Cartesian coordinates. MARS data is frequently not as high-resolution as FLUKA data, so the cubic interpolant may have greater improvement over the linear interpolant in this case.

2.2.1 Results

The interpolation for MARS data is similar to that of FLUKA. The magnet being simulated here [15] is not the same geometry as that of FLUKA, so numerical comparisons between the two are not possible. As the resolution of the MARS grid is significantly lower, it is expected that the difference between the two interpolants will be larger than in the case of FLUKA.

In fact, this is not observed significantly. The difference is still approximately 10% between the two methods at maximum. This provides good confirmation that both methods are well-conditioned for this particular problem.

Unlike in the case of the first FLUKA simulation, where the differences were approximately randomly distributed through the region of large heat load, here a definite pattern exists for the difference of the two interpolants. With the lower resolution MARS data, the two interpolants have a larger region between points in which to deviate from each other, so larger scale effects are seen. Certain artifacts present in the case of FLUKA simulations near the edge of the magnet coils are not present here.

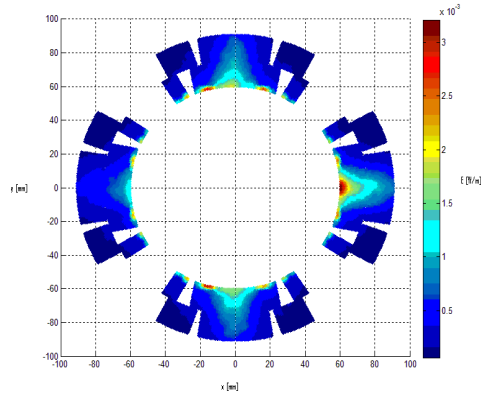


Figure 6: *Plot of result from using a bilinear interpolant on the MARS output data.*

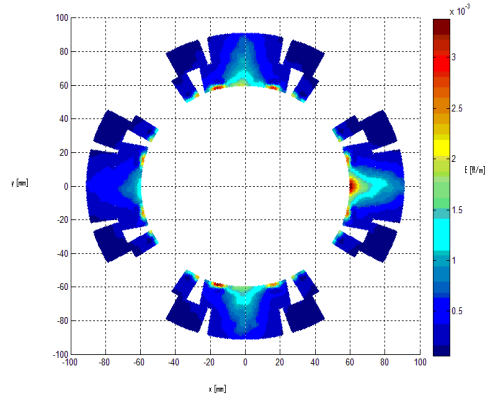


Figure 7: *Plot of result from using a bicubic interpolant on the MARS output data.*

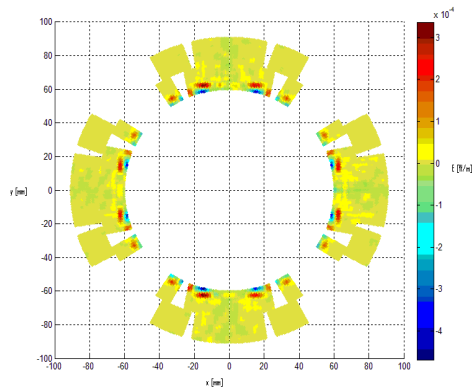


Figure 8: *Plot of the difference $L_E(r, \phi) - C_E(r, \phi)$. Note the scale difference between this and the previous two plots.*

2.3 Extension of Interpolation on FLUKA Simulations to 3-Dimensions

2.3.1 Motivation and Theory

MARS selects and returns the longitudinal bin with maximal heat load, giving the 2-dimensional energy deposit map in the most affected area. However, FLUKA's output consists of the whole 3-dimensional picture of the magnet. In order to select the most affected areas in z , a full 3-dimensional method is needed.

There are several possible ways to extend the above method to 3-dimensions. One might first think of using 3-dimensional interpolation, which is itself an obvious generalization of the 2-dimensional case. For most applications, however, only a 2-dimensional energy deposition map is needed, so this is unnecessary.

Instead, it should be acceptable to use the 2-dimensional methods on the individual cross-sections. For quench simulations, only considering those few cross-sections with the largest energy deposits should be sufficient, as these areas are most vulnerable to quenching. For this, two measures are used for what constitutes a large energy deposit—namely, the maximal energy deposit at a single point, and the total energy deposit for the whole of the longitudinal bin, i.e.

z_{max} is such that there exists $(r', \phi') \in \Lambda$ with $E(r', \phi', z_{max}) = \max_{r, \phi, z} E(r, \phi, z)$.

z_{tot} is such that $\sum_{(r, \phi) \in \Lambda} E(r, \phi, z_{tot}) = \max_z \sum_{(r, \phi) \in \Lambda} E(r, \phi, z)$.

In most cases, $z_{max} \approx z_{tot}$, as the energy deposition maps are relatively well-behaved in all three variables.

Procedure In order to use the whole 3-dimensional description of the magnet, with all longitudinal bins, the output file from FLUKA must be read in directly by the procedure. This will allow the program to find the longitudinal bin with largest heat load and create the input data corresponding to that bin to use in the 2-dimensional interpolation routines.

Data are read in assuming the standard FLUKA output file. As the data are being read in, if the integrated maximum is being searched for, the total integrated heat load in each bin is also computed. If the individual maximum is searched for, this is kept as well. From these, the program constructs a valid FLUKA input spreadsheet corresponding to the file, which can then be used for 2-dimensional interpolation. This program must be run on both the inner and outer data, which will then correspond to the same longitudinal bin, before any meaningful interpolation can be done.

3 Linearity Study

3.1 Global Tests

One hypothesis regarding the energy deposition maps is that the longitudinal bins have energy depositions linearly proportional to each other. Particularly, one would like to know given two z-bins, how close to linear is the relationship between their energy depositions. Mathematically, we want a separation of variables-type of expression, i.e. something of the form:

$$E(r, \phi, z) \approx \Omega(r, \phi) Z(z)$$

Note that if such an expression exists, then certainly many such expressions exist, as $(c\Omega(r, \phi)) \left(\frac{Z(z)}{c}\right) = \Omega(r, \phi) Z(z)$, so we may choose either Ω or Z to be normalized in some way. As such, it will be beneficial to instead consider expressions of the form

$$E(r, \phi, z) \approx k \Omega(r, \phi) Z(z)$$

for constant k , as this allows both Z and Ω to be normalized. Furthermore, it is helpful to restrict consideration to the inner cable layer of the magnet, as this is the most vulnerable to quenching.

It is easy to see that the optimal way to set Ω is by setting it as the normalized average energy deposition for that value of (r, ϕ) , i.e. $\Omega(r, \phi) = \frac{1}{n_z} \sum_{i=1}^{n_z} E(r, \phi, z_i)$, and similarly $Z(z) = \frac{1}{mn} \sum_{(r', \phi') \in \Lambda} E(r', \phi', z)$. Here, the undetermined constant of proportionality k is determined in such a way that the total energy deposition over the whole magnet is preserved, i.e. $\sum_{r, \phi, z} E(r, \phi, z) = k \sum_{r, \phi} \Omega(r, \phi) \sum_z Z(z)$.

To test how accurate this method is, it is best to normalize $Z(z)$ so that $\sum_z Z(z) = 1$. Then each data line $E(r, \phi, z)$ for all z implies a particular value for $k \Omega(r, \phi)$. We can calculate the coefficient of variation

$$\mu_\Omega(r, \phi) = \frac{\sigma_z(k_z \Omega_z(r, \phi))}{\langle (k_z \Omega_z(r, \phi)) \rangle_z}$$

of these values, which gives a measure of the variability in the model. A small coefficient of variation ($\mu_\Omega \ll 1$) indicates the model holds quite well in this case, while a larger μ_Ω suggests it does not hold.

The results from this suggested that the relation does not hold particularly well (see figure 9). The coefficient of variation ranged from about 0.5 to 0.75, which are rather large. However, an important property we observe here is that μ_Ω is not independent of position.

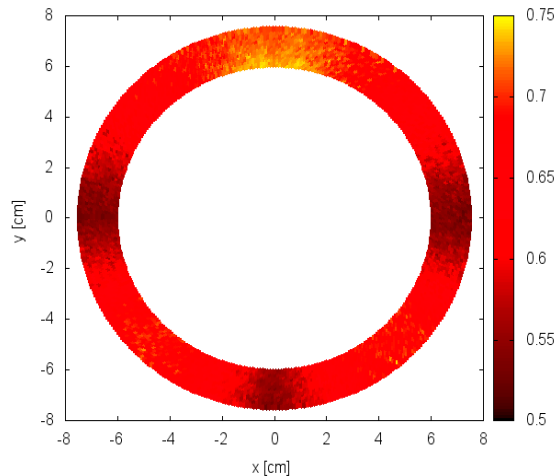


Figure 9: *Plot of μ_Ω vs. magnet position.*

In fact, an unpredicted correlation exists between the energy deposition map E and the coefficient of variation μ_Ω . The energy depositions for most cross-sections are qualitatively quite similar. All exhibit 4 maxima at the centers of the inner edges of the magnets. Three of these—here, the left, bottom, and right, are typically significantly lower in magnitude than the fourth. Here, all three of these have low μ_Ω , while the largest maximum has the highest μ_Ω .

This suggests that the model may not be exactly the same in all regions of the magnet. If this were the case, the strange behavior of μ_Ω would be easy to explain—due to the larger magnitude of data at the level of the smaller local maxima, the model fitted those points more accurately. On the other hand, the larger local maximum was an outlier, and as such had the highest variability. An easy way to test this hypothesis is to simply restrict the data set to an appropriate subset. The model will perform significantly better if this is the case.

3.2 Local Studies for Linearity

3.2.1 Maximal Study of Variability in Linear Model

It is conceivable that the failure of the above model is because different parts of the coil must be fit differently. If this is the case, there are a number of ways to test such a hypothesis. The first is to only consider a small number of (r, ϕ) values in the same part of the magnet. The most interesting part of the magnet is near the maximal heat deposits, and correspondingly this also has the lowest associated error in the FLUKA calculation. As such, it makes sense to restrict to some small number of (r, ϕ) where the energy deposits are maximized; in practice these are almost all in the same region of the magnet.’

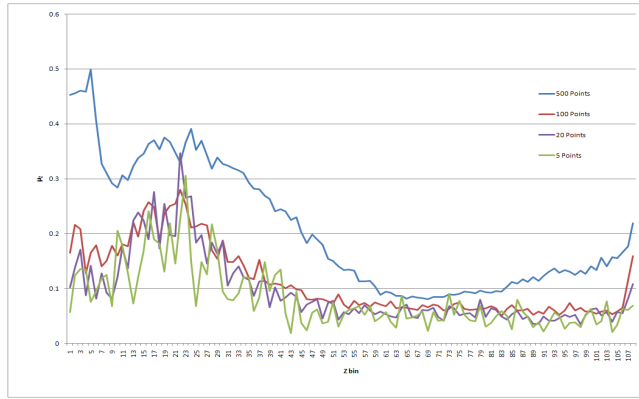


Figure 10: Plot of μ_Z vs. z for different numbers of (r, ϕ) points. There are a total of 14 bins in r and 384 in ϕ ; 500 bins represents approximately 9.3% of the magnet.

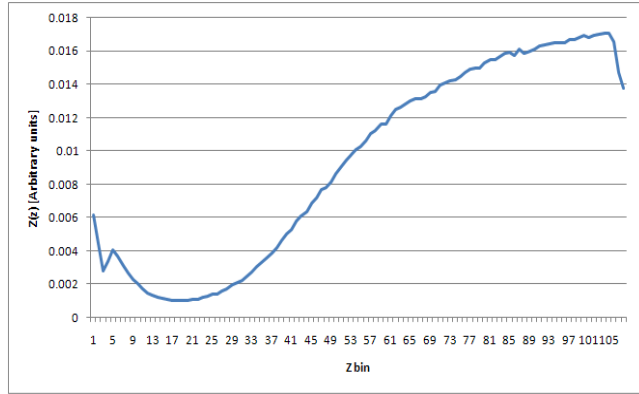


Figure 11: Plot of $Z(z)$ vs. z . The scale on the vertical axis is arbitrary. Note that the maximum corresponds to areas of low variation in figure 10.

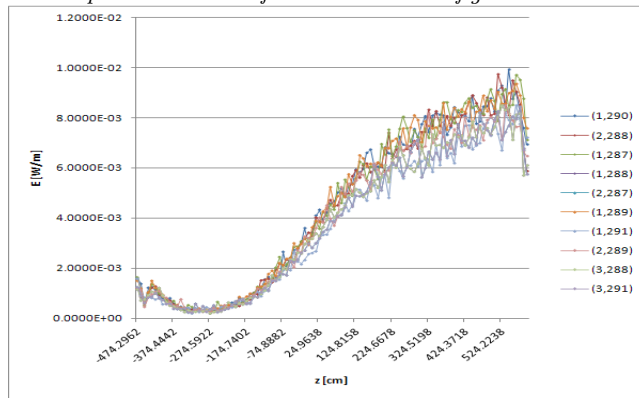


Figure 12: Plot of $E(z)$ vs. z for the 10 values of (r, ϕ) with maximal E . Qualitatively, this appears to have the desired form.

We recall that there are two possible measures for what (r, ϕ) values have maximal energy deposit—the absolute and the integrated measure. Previously, the maximal value in z was found; here the same procedures are used to find maxima in (r, ϕ) . These give almost exactly the same results in all cases, so it will be sufficient to consider only the integrated measure for energy deposit, which behaves slightly better with random errors.

Figure 10 shows how the longitudinal coefficient of variation μ_Z behaves vs z for 5, 20, 100, and 500 values of (r, ϕ) corresponding to the largest integrated energy deposits. μ_Z is defined analogously to μ_Ω , but measures the variability as a function of z instead of as a function of r and ϕ . Comparing with figure 11, it is clear that the separation of variables performs better at larger energy depositions, which is thought to be due to random errors constituting a larger fraction at smaller energy depositions. It is not a problem, however, as the region of interest is conveniently precisely where the energy depositions are large.

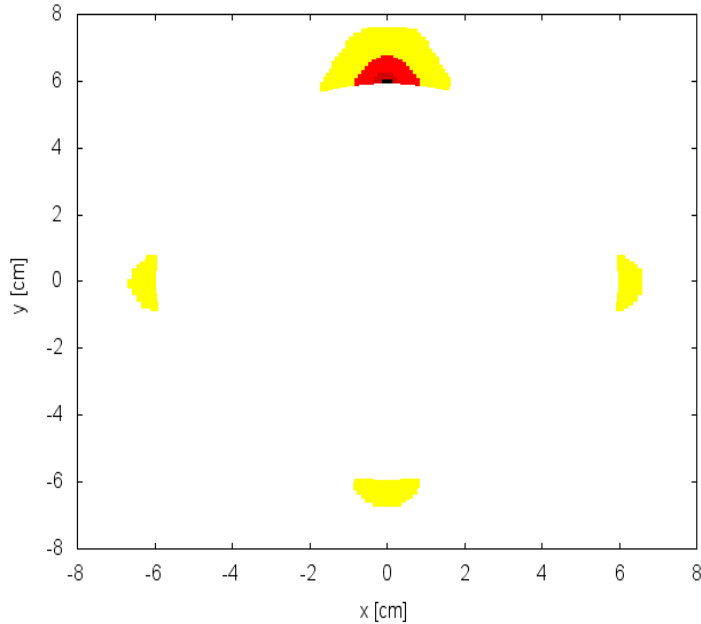


Figure 13: Plot of (r, ϕ) points chosen by the method. Here black corresponds to points 1-5, brown to 6-20, red to 21-100, and yellow to 101-500. Note that all the points not in the upper pole are yellow.

An unwanted phenomenon is observed as the number of (r, ϕ) points increases. Some of the points begin to fall outside the desired pole of the magnet. In figure 13, it is clear that the method begins choosing points outside the desired pole between 100 and 500 points. This may correspond to the substantial increase in μ_Z for 500 points over 100 points. To alleviate this, the simplest method is to restrict to points inside the desired pole.

3.2.2 Restricting to One Quadrant

Restricting to one pole can be done entirely by eliminating data with the incorrect bins in ϕ . For the top pole, $\frac{\pi}{4} < \phi < \frac{3\pi}{4}$, which corresponds to the pole with the observed maximum energy deposit. Figure 14 shows the points chosen once restricted to the desired pole. The 500 points chosen represent over 38% of the pole, and constitute significantly more than half of the energy deposition in the pole.

It is notable that this restriction is justified from a practical perspective. The poles are separated by cooling channels, which effectively stop a quench from advancing to the other poles. There is little heat interaction between the poles due to these channels. As such, simulations of the individual poles are sufficient to describe the dynamics.

Figure 15 compares the the restricted and unrestricted methods for 500 points—the only case where they disagree. The results for the restricted method are somewhat better than the unrestricted method. μ_Z did decrease in most cases, but the decrease was not particularly drastic. μ_Z remains at the 10% minimum level, but this method increases the range in which the separation of variables is accurate.

The improvement is not as good as expected, which supports the alternate theory that the variation is caused by random fluctuations associated with the model, which are more significant at smaller energy deposition levels—as more points are added, this effect will eventually dominate the variability, limiting the range in which it is accurate. This is not expected to cause major problems since one can easily extrapolate to the points of lower energy depositions, which are less significant in quench studies.

3.3 Additional Test by Comparison of Different Z-bins

3.3.1 Full Cross-sectional Comparison

The above material may be enough to justify the model numerically, but demonstrations of the accuracy in particular cases are desirable to validate the methodology. In particular, this will be useful to determine how accurate such an approximation may be in practice, based on more familiar measures of variability. The error can be analyzed on the basis of individual bins, rather than averaged over the entire magnet.

One way to do this is to make a scatter plot of the energies in 2 separate z-bins. If the expression holds, i.e. $E(r, \phi, z) = \Omega(r, \phi) Z(z)$, then we must have $\frac{E(r, \phi, z_1)}{E(r, \phi, z_2)} = \frac{Z(z_1)}{Z(z_2)}$ a constant. So we expect that for any z_1, z_2 , the plot of $E(r, \phi, z_1)$ vs $E(r, \phi, z_2)$ for all (r, ϕ) should be linear in nature.

Figure 16 shows this correspondence for 8 randomly selected pairs of longitudinal bins. There are several interesting trends that are observed in these and other plots. These plots confirm the prediction of the previous method that the linear behavior is more closely followed at higher energy depositions. For instance, in the plot of bin 101 against 103—two of the bins with the highest

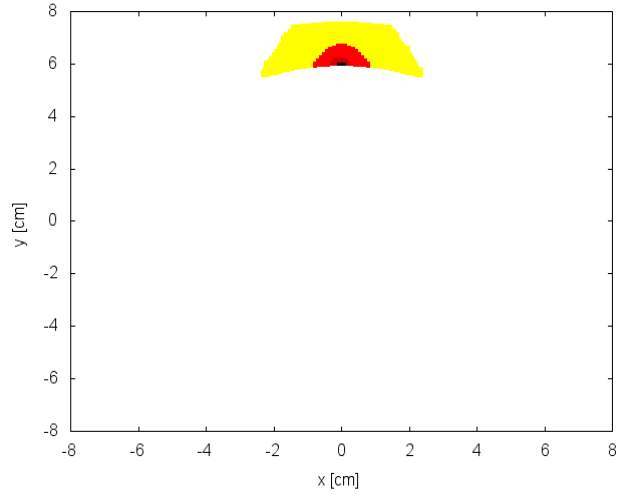


Figure 14: Plot of (r, ϕ) points chosen by the method after restricting to the top pole. Here black corresponds to points 1-5, brown to 6-20, red to 21-100, and yellow to 101-500.

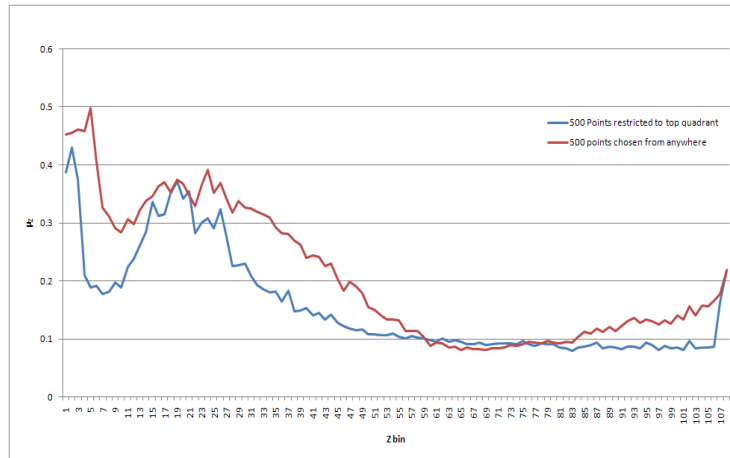


Figure 15: Comparison of μ_z for unrestricted and restricted methods. The red curve is the same as in figure 10, while the blue uses the data restricted to the top pole.

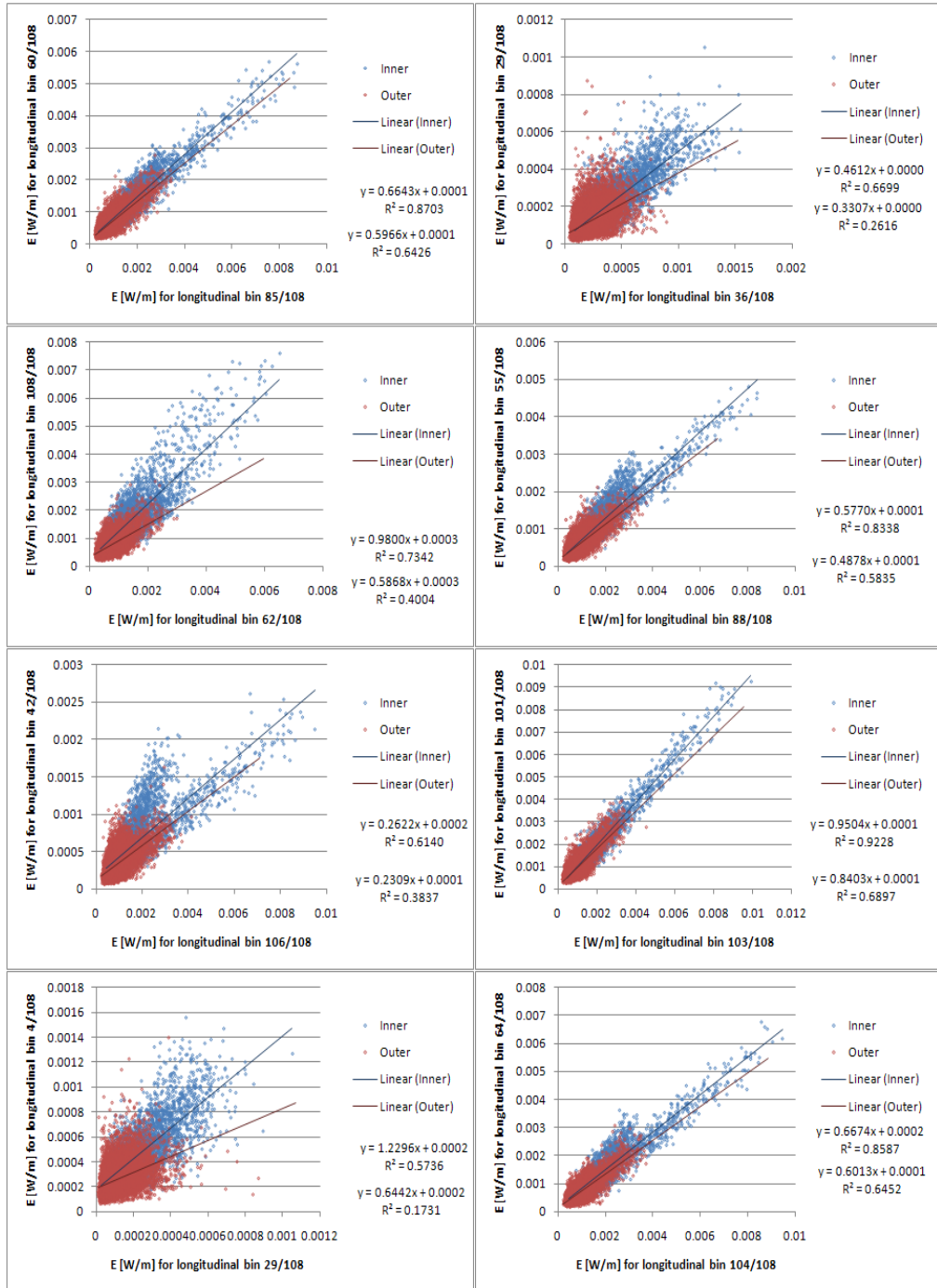


Figure 16: Comparisons of energy depositions in 8 randomly selected pairs of longitudinal bins. Note that the linearity improves at higher energy depositions.

energy deposition—the observed R^2 value for the inner coils is approximately 0.92. By contrast, in the plot of bin 4 against bin 29, the R^2 value for the inner part of the magnet is only 0.57, suggesting departure from the model. The R^2 values for the outer part are consistently lower than for the inner part, again agreeing with expectations. Qualitatively, one can also see in several plots that the data cluster near the regression line much more closely at the higher energy deposits than at lower energy deposits.

A major problem with these plots is the problem of regression dilution. The regression lines given are optimal assuming no variance exists in the independent variable. This is not the case here, and thus if the slopes of the regression lines were used to predict the quotient $\frac{Z(z_1)}{Z(z_2)}$, this would lead to an attenuation bias. The practical effect is that the correspondence, and consequently the slope of the regression line, is always underestimated, and consequently the y-intercept is always overestimated. This effect is stronger at lower R^2 values, explaining why the outer coils consistently have a lower slope than the inner coils. It is possible to correct for attenuation bias or to use regression methods which are symmetric in independent and dependent variables, but these have other associated undesirable features. The main object of interest is not the value of $\frac{Z(z_1)}{Z(z_2)}$, which can easily be calculated by other methods, but the accuracy of the approximation, given by the R^2 value, which is symmetric in the variables.

The best R^2 value shown is about 0.92, which corresponds to a coefficient of determination of about 0.96. However, in many other cases the results are not as close to the desired value of $R^2 = 1$. Part of the reason for this is the inclusion of the whole cross-section. One might think that including only points in the inner cable layer of the magnet in one pole, and restricting to those (r, ϕ) with large energy deposits, would produce better results, as in the previous case.

3.3.2 Restricted Comparisons

As before, data are restricted to the top pole, which exhibits the largest energy depositions. One pole represents 96 bins in ϕ in the FLUKA, each corresponding to 14 bins in r . For the value of (r, ϕ, z) with maximal energy deposit, keeping r and z constant and varying ϕ , it is found that $E(r, \phi, z)$ has decreased by a factor of 2 approximately 10 bins in each direction from the maximum. As such, only the ϕ values between 1.415217 and 1.775181 are kept, corresponding to bins 279 to 301 out of 384. With this, approximately 8% of the magnet is used.

Surprisingly, this is not observed. Figure 17 shows the results of regression on this reduced data set for the same cases as figure 16. The R^2 values in the cases where the regression worked well previously show slight improvement. However, in most of the cases where it worked poorly before, there is little improvement, and in some cases a reduction in accuracy. One explanation is that the data have gotten narrower in extent due to the restriction, which would reduce the R^2 value. Previously, the energy deposits got near 0; now their lower bounds are approximately 25% of the upper bound, suggesting a reduced extent along

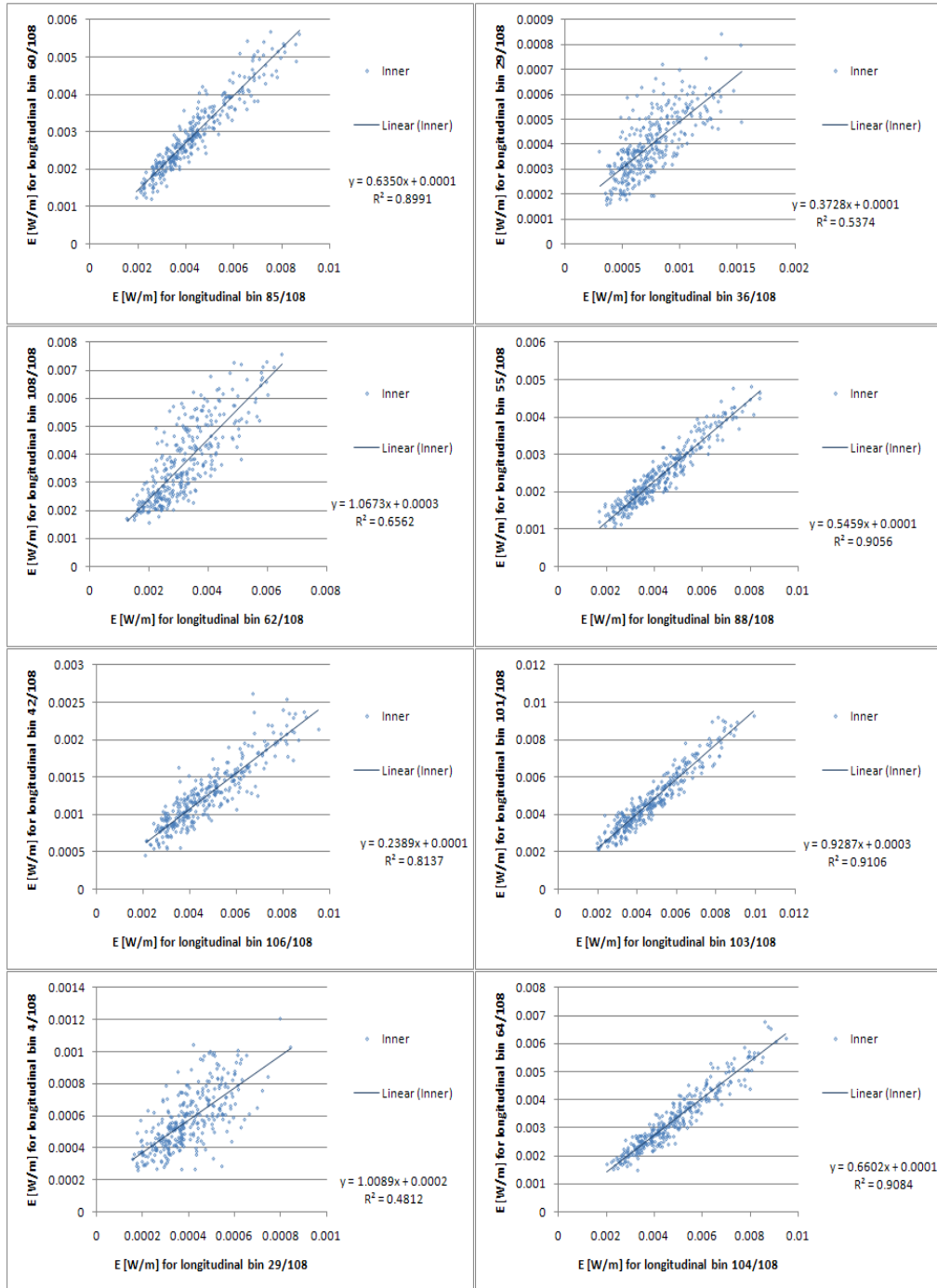


Figure 17: Comparisons of energy depositions in 8 randomly selected pairs of longitudinal bins after restricting to the top pole near the largest energy deposits. The data do not show significant improvement over the original unrestricted comparisons.

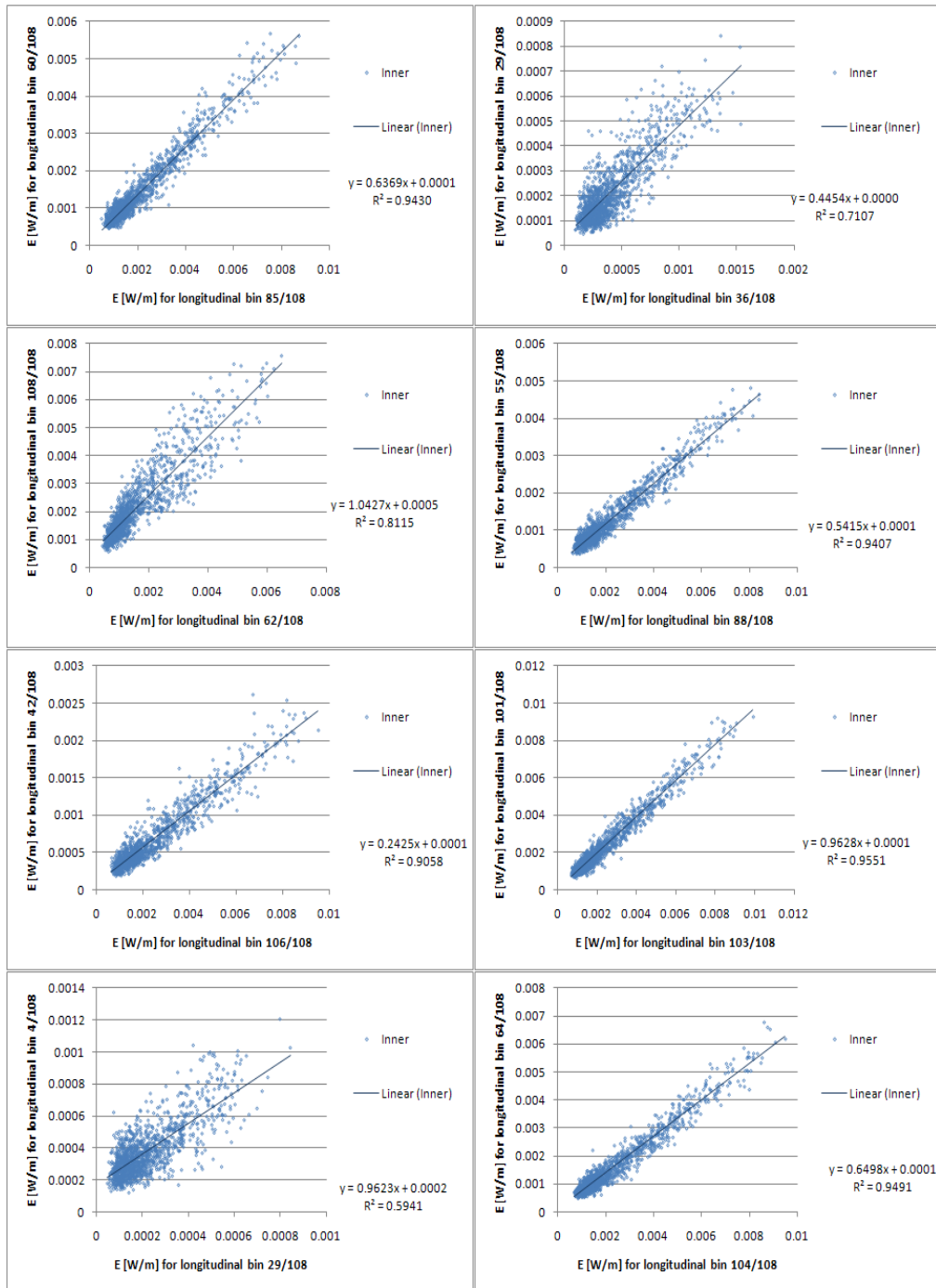


Figure 18: Comparisons of energy depositions in 8 randomly selected pairs of longitudinal bins after restricting to the entire top pole. Unlike in figure 17, here there is significant improvement.

the axis of dependence.

Figure 18 confirms that this is the likely explanation—plots after restricting to the top pole, but no further, show significant improvement in general over both of the previous plots. These extra data points near the origin provide confirmation of the model rather than add variability, seemingly contradicting previous results. However, two different meanings of variability are implied—in the previous method, the variability was inversely proportional to the mean energy, while here it is independent of mean energy.

Both measures of variability appropriate in different contexts; when studying and computing values of $Z(z)$ or modeling the most sensitive portions of the magnet, μ_Z is the most important measure, but when modeling all of a particular cross-section, the R^2 measure is more useful. This is supported by the existence of regression dilution, which implies that computation of values of $Z(z)$ through regression will be inaccurate, and that the optimal method is through the averaging done in section 3.1. One could correct for the attenuation bias, but doing so is complicated and error-prone, requiring multivariate statistics, and provides no significant advantages over the averaging method.

4 Conclusions

Bilinear and bicubic interpolation methods were used to interpolate the energy deposition maps onto the coordinates of the conductors. Both the interpolation methods have been tested and demonstrated useful for both FLUKA and MARS data. The fact that they agree to within about 10% provides confirmation of the success. In particular, they will not add significant additional error to the energy deposition calculations, which already have intrinsic error associated with MARS or FLUKA.

This will be useful in the future. The network model allows computation of magnet limiting conditions, which depend on external factors as well as the energy deposits. The interpolation routines will provide the necessary interface between the FLUKA and MARS simulations, which work in one coordinate system, and the network model, which uses a different coordinate system. It is thus an important component in quench protection, and the accuracy displayed helps reduce the uncertainty in the model.

Approximate linearity in the cross-sectional energy deposition maps was demonstrated. In particular, in the regions of interest, i.e. those of large energy deposits, the linearity is followed quite closely. In areas of lower energy deposition, the intrinsic errors from FLUKA are higher, so to a good approximation the linearity is held.

This result may prove useful in a number of ways in the future. Simulations like FLUKA could possibly be simplified by making such an approximation. This would allow for faster and more accurate simulations. Alternatively, with more data, one could conduct analysis on the component parts of the energy deposition map, $\Omega(r, \phi)$ and $Z(z)$. Tests of linearity over a different type of magnet, such as a dipole, could also be done. This would give an idea when the

approximation is accurate, and how it breaks down.

References

- [1] LHC Design Report, The LHC main ring, vol. 1, CERN-2004-003.
- [2] V. L. Ginzburg, E. A. Andryushin, *Superconductivity*, Revised Edition, ISBN 981-238-913-X.
- [3] M. N. Wilson, *Superconducting Magnets*, ISBN 0-19-854805-02, 1983.
- [4] J.B. Jeanneret et al., Quench levels and transient beam losses in LHC magnets, LHC Project Report 44, CERN, 1996.
- [5] 'The MARS Code System Users Guide', N.V. Mokhov, Fermilab-FN-628 (1995). <http://www-ap.fnal.gov/MARS/>.
- [6] 'MARS15 Overview', N.V. Mokhov, S.I. Striganov, Fermilab-Conf-07/008-AD (2007); in Proc. of Hadronic Shower Simulation Workshop, Fermilab, September 2006, AIP Conf. Proc. 896, pp. 50-60 (2007). 'Physics Models in the MARS15 Code for Accelerator and Space Applications', N.V. Mokhov, K.K. Gudima, S.G. Mashnik et al, in Proc. of International Conference on Nuclear Data for Science and Technology, Santa Fe, NM, 2004, AIP Conf. Proc. 769, part 2, pp. 1618-1623; Fermilab-Conf-04/269-AD (2004).
- [7] 'The physics models of FLUKA: status and recent developments', A. Fasso', A. Ferrari, S.Roesler, P.R. Sala, G. Battistoni, F. Cerutti, E. Gadioli, M.V. Garzelli, F. Ballarini, A. Ottolenghi, A. Empl and J. Ranft, Computing in High Energy and Nuclear Physics 2003 Conference (CHEP2003), La Jolla, CA, USA, March 24-28, 2003, (paper MOMT005), eConf C0303241 (2003), arXiv:hep-ph/0306267
- [8] 'FLUKA: a multi-particle transport code', A. Fasso', A. Ferrari, J. Ranft, and P.R. Sala, CERN-2005-10 (2005), INFN/TC_05/11, SLAC-R-773
- [9] "Modeling of Quench Limit for Steady State Heat Deposits in LHC Magnets" D. Bocian, B. Dehning, and A. Siemko, IEEE Trans. Appl. Supercond. 18, 112 (2008).
- [10] "Quench Limit Model and Measurements for Steady State Heat Deposits in LHC Magnets", D. Bocian, B. Dehning, and A. Siemko, IEEE Trans. Appl. Supercond. 19, 2446 (2009).
- [11] "ROXIE: Routine for the optimization of magnet X-sections, inverse field calculation and coil end design," in Proceedings of the First international ROXIE Users Meeting and Workshop, S. Russenschuck, Ed., Geneva, Switzerland, March 1998.

- [12] S. Russenschuck, *Electromagnetic Design and Mathematical Optimization Methods in Magnet Technology*, 3rd ed., ISBN 92-9083-242-8, www.cern.ch/russ, 2006.
- [13] William Press, Saul Teukolsky, William Vetterling and Brian Flannery, *Numerical Recipes. The Art of Scientific Computing*, 3rd Edition, ISBN 0-521-88068-8, 2007. (C++ code), section 3.3.6
- [14] 'Inter-comparison of MARS and FLUKA: Predictions on Energy Deposition in LHC IR Quadrupoles', C. Hoa, N. Mokhov, F. Cerutti, A. Ferrari, LHC-Project-Note-411, February 2008.
- [15] V.V. Kashikhin et al., Performance of Nb3Sn Quadrupole Magnets under Localized Thermal Load, CEC/ICMC2009, Tucson, AZ, 2009.